

Molecular dynamics simulation of the production of acoustic waves by pulsed laser irradiation

J. I. Etcheverry*

Departamento de Matemática, Facultad de Ciencias Exactas y Naturales, Universidad de Buenos Aires, Pabellón I, Ciudad Universitaria, 1428 Buenos Aires, Argentina

M. Mesaros

Departamento de Física, Facultad de Ingeniería, Universidad de Buenos Aires, Paseo Colón 850, Buenos Aires, Argentina

(Received 8 January 1999)

In this work we model the production of acoustic waves in a material irradiated by a pulsed laser, by means of molecular-dynamics simulation. We show that with this technique and using a simple Lennard-Jones interaction potential, quantitative information on the acoustic waves is obtained for a wide range of laser energies. Results for laser fluences producing heating and even melting and ablation of the irradiated material are presented, thus extending what can be obtained by means of the standard thermoelastic models. Moreover, we show that at low fluences the obtained results are in very good agreement with standard thermoelastic calculations. [S0163-1829(99)01437-X]

I. INTRODUCTION

The use of pulsed lasers to produce high-frequency acoustic pulses in both liquid and solid media has been demonstrated to be a very useful tool in many areas of applied science, mainly in nondestructive evaluation and materials characterization.¹⁻⁶

The production of acoustic waves in metals irradiated with low fluence laser pulses is mainly associated with the production of thermal stress inside the material.^{2,4,7,8} The theoretical analysis of the coupling between the heating of the material produced by the laser and the stress produced by thermal dilatation has been extensively studied, both from the analytical^{2-4,8-11} and the numerical viewpoints.¹²

However, the analysis is much more difficult when melting and ablation take place, because there are many nonlinear phenomena involved.⁸ For instance, important changes in specific volume and thermal and elastic properties are produced when the material melts. Also, the latent heats of melting and vaporization must be taken into account, and at high laser powers the recoil pressure exerted by the evaporated material is a dominant process in the production of acoustic waves. Hence, evaporation and ablation must be carefully accounted for. In addition, for subnanosecond irradiation, nonequilibrium phenomena like cluster expulsion play a significant role.¹³

Standard methods based on thermoelastic equations are not well suited for the analysis of the very involved mathematical problems that arise when melting and ablation take place, because of the appearance of free boundaries (solid-liquid, liquid-vapor) and too many nonlinearities to be taken into account.

In this framework, molecular dynamics simulations have from the mathematical viewpoint the advantage of including the nonequilibrium behavior. Also free boundaries appear naturally, without requiring a separate treatment of melted and solid parts of the irradiated sample. According to the details of the interaction potential used, nonlinearities like

the melting and vaporization latent heats, and dependence of thermal and elastic constants with temperature are automatically taken into account.

The main drawback is the very high computational cost, because to study the production of acoustic waves macroscopic domains are required. This also limits the accuracy of the interaction potentials that can be used. However, the advance in computing power is bringing into the reach the calculation of systems of hundreds of millions of particles.¹⁴⁻¹⁷

In this work we demonstrate that meaningful and interesting results can be obtained by means of a molecular dynamics simulation of 5×10^5 particles interacting by a simple Lennard-Jones potential. We want to emphasize that the calculations were performed in a desktop PC (Pentium II 400 MHz). We also show that the molecular dynamics results are in very good agreement with standard thermoelastic techniques for small laser fluences.

This work is organized as follows: we first describe the molecular dynamics technique, and present some numerical results showing how the variables of interest are recovered by averaging from the molecular dynamics information, and finally the comparison with standard thermoelastic techniques. Further work analyzing in detail many other aspects of the irradiation process (cluster ablation, surface melting detection, etc.) is currently in progress, and will be reported elsewhere.

II. ALGORITHM

The basic problem involved is the solution of the Newton equations for each particle, interacting with its neighbors by means of a pairwise Lennard-Jones force:

$$m_i \frac{d^2 \mathbf{x}_i}{dt^2} = \sum_{j \neq i} \mathbf{F}_{i,j}, \quad (1)$$

where m_i and \mathbf{x}_i are the mass and position of the particle i respectively, and the interaction force between particles i and j , $\mathbf{F}_{i,j}$, is obtained from the shifted Lennard-Jones potential:

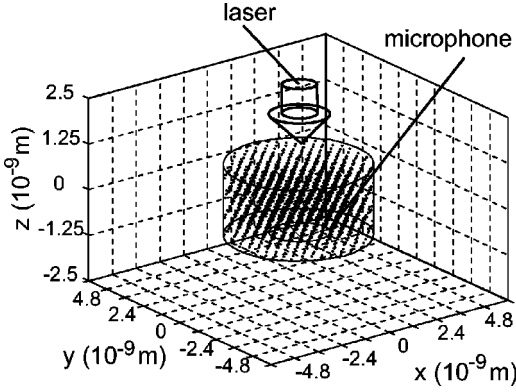


FIG. 1. Schematic diagram of a typical irradiation geometry, with a small initial lattice. The computational division in cells is shown on the axis. The particles used to detect the acoustic waves are identified as microphone.

$$V(\mathbf{x}_i, \mathbf{x}_j) = \begin{cases} V_{LJ}(r) - V_{LJ}(r_c) & r \leq r_c \\ 0 & r_c < r, \end{cases} \quad (2)$$

where V_{LJ} stands for the Lennard-Jones potential:

$$V_{LJ}(r) = 4\epsilon \left[\left(\frac{\sigma}{r} \right)^{12} - \left(\frac{\sigma}{r} \right)^6 \right]. \quad (3)$$

$r = \|\mathbf{x}_i - \mathbf{x}_j\|$ is the interparticle distance, and r_c is the assumed cutoff of the potential. In all simulations presented in this work, we use $r_c = 2.5\sigma$ and parameters for the Lennard-Jones potential corresponding to argon Ar,¹⁸

$$\epsilon = 119.8k \text{ (K)}, \quad \sigma = 3.406 \text{ \AA}$$

(k is the Boltzmann constant).

The calculations are organized by means of a cell list approach¹⁹ in order to avoid the calculation of the interaction between particles located farther away than the cutoff radius. The computational domain is divided in small cells, of linear dimensions of the order of the cutoff radius r_c . A linked list pointing to the particles in each cell is generated at each time step, and used to compute the interactions. Only interactions between particles in adjacent cells are considered. The particles are then advanced in time by means of the explicit Verlet algorithm.^{18,20} The main advantage of this approach is that the problem size grows linearly with the number of particles considered, thus allowing the computation of large systems, of the order of 500 000 particles in the simulations presented here. The runs were performed in a desktop PC and took 4 h each, on average.

The assumed boundary conditions are free, i.e., there are no restrictions on the particles or the temperature at the boundary. In this way, the simulations correspond to the problem of the irradiation of a small block of material in vacuum. In particular, we will see that this enforces the use of large domains, in order that the reflections of the acoustic wave do not mask the true form of the acoustic pulse.

The particles were initially located on an fcc lattice, which in some simulations was cut with the form of a solid cylinder, as shown in Fig. 1. Notice also the division in cells of the computational domain, and the assumed laser irradiation geometry.

The initial velocities were given at random, with a Gaussian distribution corresponding to the desired temperature. In the simulations presented here the initial temperature was assumed to be 50 K. The samples were initially thermalized for 100 ps (with time steps of 25 fs).

In order to minimize the subsequent oscillations of the sample, the lattice parameter must be chosen carefully for the desired temperature. This is a critical issue, because we want to be able to detect very small acoustic signals, and even a small error in the lattice parameter causes strong oscillations that take a prohibitively long time to damp out. We have adopted several strategies to overcome this difficulty, from simply integrating in time until oscillations are damped out by interference, to more sophisticated techniques simulating a thermal bath.²¹ The most simple and successful strategy consisted in averaging the normal position over a whole disk in the rear surface of the sample in order to reduce the random noise, and using an accurate expression for the nearest-neighbor distance in the solid phase. For instance, in three dimensions we used the expression

$$r_s(T) = 1.0964 + 0.054792T + 0.014743T^2 + 0.083484T^3 - 0.23653T^4 + 0.25057T^5 \quad (4)$$

given by Broughton *et al.*,²² where r_s and T are given as usual in units of σ and ϵ . The disk used to detect the acoustic waves is indicated as microphone in Fig. 1 to stress the analogy with a typical acoustic wave generation experiment.

The laser irradiation was modeled assuming a pulse that is Gaussian in time, incident normally on the sample (see Fig. 1). We used time durations of the order of 5 ps, and uniform irradiation profiles, in order to simulate an essentially one-dimensional (1D) geometry, where results are easily compared to the numerical solution of a more detailed 1D model (see Sec. IV).

The laser energy coupling inside the material was simulated distributing the laser energy cell by cell, by multiplying the velocities of all the particles in each cell by an adequate factor. The amount of energy deposited in each cell is calculated by means of Beer's law:

$$\frac{dI}{dz} = -\mu I(r, z), \quad (5)$$

where I is the laser intensity in the location (r, z) , and the absorption coefficient μ is assumed to be proportional to the material density. In the simulations presented the absorption coefficient was chosen in such a way that the penetration depth inside the material was of the order of tens of nm.

A different approach to the energy deposit problem is the introduction of an electronic temperature satisfying a heat equation with a source term due to the incoming laser energy, and with a coupling term to the lattice dynamics. This approach has been used in molecular dynamics simulations of point defects production by irradiation of a material,^{23,24} and in the molecular dynamics study of surface melting of copper samples,²⁵ for instance. However, we have found that the basic mechanism used to couple the electronic temperature to the lattice dynamics produces a non-negligible damping of the acoustic waves. In fact, this technique has been

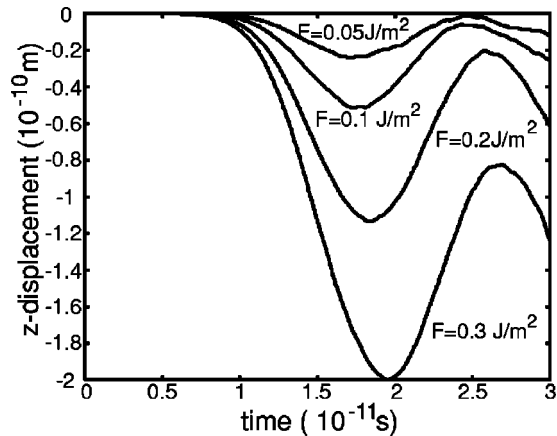


FIG. 2. Vertical displacement of the bottom of the irradiated sample, showing the arrival of the acoustic longitudinal pulse. Pulse duration: 5 ps full width at half maximum (FWHM), centered at $t = 10$ ps.

used in investigations of fracture dynamics^{21,16} to efficiently damp out the outgoing acoustic waves, and is therefore not used in our work.

Some care is required, also, in the velocity scaling procedure. In fact, if the velocities of all particles are simply scaled in order to increase the cell kinetic energy to the new desired value, collective motions are unduly amplified. In order to avoid this artifact, we subtracted the average velocity of the cell before scaling. In this way only the true random movement is amplified, and not the net mass flow.

III. MOLECULAR DYNAMICS RESULTS

In this section we present results of the molecular dynamics simulations, showing the obtained shape of the longitudinal acoustic waves, for uniform irradiation conditions. The sample used is a $91 \times 181 \times 31$ atoms lattice, with lateral dimensions much larger than the depth (to give practically one-dimensional behavior when irradiated with a spatially uniform laser pulse). The physical dimensions of the domain, assuming parameters corresponding to argon, are slightly smaller than the dimensions of the computational domain, of about $52 \times 52 \times 10$ nm³. When particles evaporated from the sample reach the boundary of the computational domain, they are dismissed. Accounting for the number of evaporated particles, and for the momentum carried away, we have a simple and precise means of detecting ablation thresholds.

The ‘‘microphone’’ used to detect the acoustic waves was a disk of 10^{-8} m radius, and two atomic layers wide. The two atomic layers were chosen to be the second and third layers from the bottom of the sample (in order to avoid the noise introduced by the eventual vaporization of some atoms in the bottom layer).

In Fig. 2 we show the z component of the displacement registered for irradiation with a spatially uniform Gaussian in time pulse of 5-ps duration, and fluences 0.05 J/m², 0.1 J/m², 0.2 J/m², and 0.3 J/m². The first three of these fluences are below, very close, and above the melting threshold, respectively. The last one is well beyond the onset of ablation. The Gaussian laser pulse peaks at a time of 10 ps in these simulations.

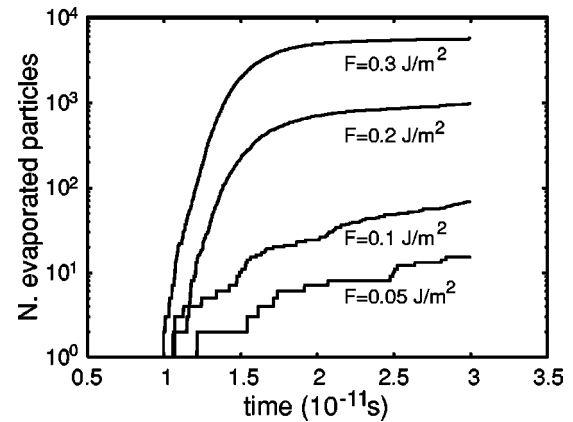


FIG. 3. Number of evaporated particles, as a function of time. Pulse duration: 5 ps FWHM, centered at $t = 10$ ps.

The number of particles that leave the computational domain as a function of time, for the previous irradiation fluences, is shown in the Fig. 3. We observe that at higher fluences the curve is steeper a short time after firing the laser. The delay relative to the laser pulse is associated with the time of flight between leaving the surface of the irradiated slab, and reaching the edge of the computational domain. This is more clearly seen in Fig. 4 where the rate of particle loss is plotted against time. At low fluences (0.05 J/m² and 0.1 J/m²) the evaporation rate is very small. At higher fluences (0.2 J/m² and 0.3 J/m²) we observe an ablation pulse that almost follows the laser pulse. This supports the idea that ablation occurs mainly during the laser pulse, and not as a result of the ulterior destabilization of the irradiated volume.^{26–28} The distortion of the ablation pulse shape with respect to the original Gaussian laser pulse is due to a variety of causes. For instance, the different times of flight between fast and slow particles produce the long tail of the evaporation pulse. The same effect is produced by the fact that particles have a nonzero velocity component along the surface. Finally, some destabilization effect with characteristic time of the order of a few picoseconds could be at play.

In order to understand better the evaporation phenomena, we plot in Fig. 5 the z component of the momentum carried away by the evaporated particles. The time derivative of this magnitude gives essentially the recoil force that the surface of the material is suffering by evaporation. The results are

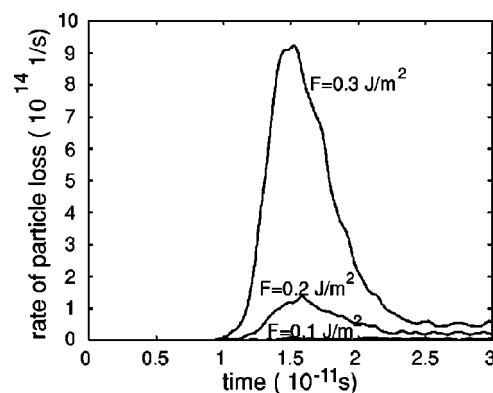


FIG. 4. Rate of particle loss as a function of time. Pulse duration: 5 ps FWHM, centered at $t = 10$ ps.

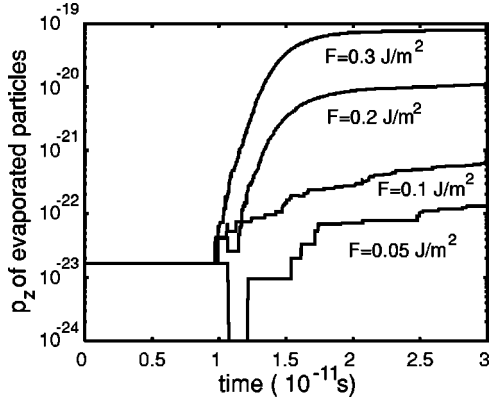


FIG. 5. Normal component of the momentum loss as a function of time. Pulse duration: 5 ps FWHM, centered at $t = 10$ ps.

plotted in Fig. 6. The standard theoretical means of accounting for the contribution of the pressure of the evaporated material to the production of acoustic waves consists of modeling in some way the recoil force.^{1,4} Figure 5 suggests that this force can be accurately modeled as the convolution of the laser-pulse shape with a decaying exponential, with a characteristic time of the order of a couple of picoseconds. Further work extending this numerical evidence to more general pulse shapes is currently in progress.

IV. THERMOELASTIC REGIME

The thermoelastic mechanism, which is usually the principal responsible for the production of acoustic waves upon laser irradiation, has been extensively studied from the theoretical viewpoint in the linear regime.^{1,3,4,7,9-11,29} The most usual model consists of the solution of the heat equation, to describe the increase of the temperature due to the incoming laser energy, and of the solution of the linear elasticity equations, with a term of coupling with temperature:

$$\rho c_p \frac{\partial T}{\partial t} = \nabla[\kappa(T)\nabla T] + Q(x,t), \quad (6)$$

$$\rho \frac{\partial^2 \mathbf{u}}{\partial t^2} = \rho c_t^2 \Delta \mathbf{u} + \rho(c_l^2 - c_t^2) \nabla(\nabla \cdot \mathbf{u}) - K\alpha \nabla T, \quad (7)$$

where T is the sample temperature and \mathbf{u} is the vector of displacements. ρ , c_p , and κ are the density, the specific heat,

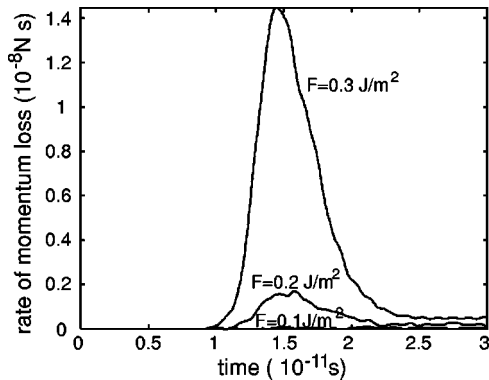


FIG. 6. Rate of the z -momentum loss as a function of time. Pulse duration: 5 ps FWHM, centered at $t = 10$ ps.

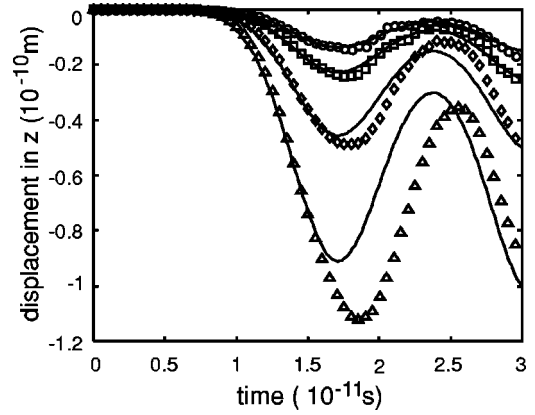


FIG. 7. Comparison between the displacements in z registered by molecular dynamics simulations (symbols) and that obtained by solving the linear thermo-elastic equations (solid line), for several laser fluences. \circ , 0.03 J/m^2 ; \square , 0.05 J/m^2 ; \diamond , 0.1 J/m^2 ; \triangle , 0.2 J/m^2 .

and the thermal conductivity, respectively. c_l and c_t are the velocities of the longitudinal- and transverse-acoustic waves, K is the modulus of cubic compressibility, and α is the thermal coefficient of volume expansion. $Q(x,t)$ represents the energy flux due to the laser irradiation.

Assuming a laser spot much larger than the characteristic thickness of the sample, we can approximately consider the problem as being one dimensional. In this 1D setting, the relevant Eqs. (6) and (7) can be written as

$$\rho c_p \frac{\partial T}{\partial t} = \frac{\partial}{\partial z} \left(\kappa(T) \frac{\partial T}{\partial z} \right) + Q(z,t), \quad (8)$$

$$\rho \frac{\partial^2 u}{\partial t^2} = \rho c_l^2 \frac{\partial^2 u}{\partial z^2} - K\alpha \frac{\partial T}{\partial z}, \quad (9)$$

where now u is the z component of the displacement vector \mathbf{u} .

The boundary conditions corresponding to nonexistence of stresses at the boundary surfaces are, within the same linear approximation,

$$-\frac{TK\alpha}{\rho} + c_l^2 \frac{\partial u}{\partial z} = 0. \quad (10)$$

Assuming a Gaussian in time laser pulse impinging normally on the surface located at $z = z_0$, we have

$$Q(z,t) = A\mu I_0 \exp[-(t-t_0)^2/\tau^2 - \mu(z-z_0)], \quad (11)$$

where A is the absorptivity (fraction of the undisturbed laser energy I_0 that actually penetrates into the material), μ is the absorption coefficient, τ is the laser pulse width, and t_0 is the time where the laser intensity is at maximum.

In order to compare the solutions obtained by molecular dynamics with those of the linear thermoelastic model, we solved numerically the previous equations in a domain of the same dimensions of that used for the molecular dynamics simulations. The comparison between the acoustic waves obtained with these two approaches is shown in Fig. 7. We see that at low fluences (0.03 J/m^2 and 0.05 J/m^2) the curves are very similar, but that for higher fluences the results are pro-

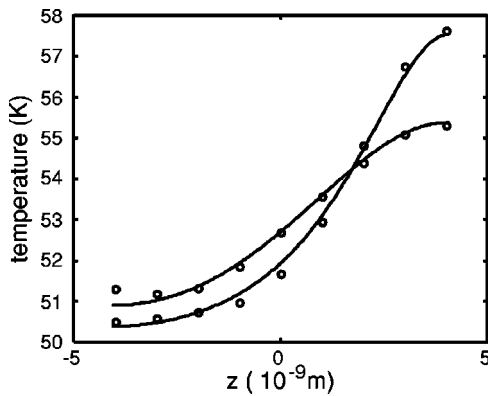


FIG. 8. Temperatures at $t=15$ ps and $t=30$ ps, obtained by molecular dynamics (circles) and linear thermoelasticity (solid line). Laser fluence: 0.03 J/m^2 .

gressively different. This behavior is produced, for fluences below the melting threshold, mainly due to the temperature dependence of the physical constants of the Lennard-Jones solid (at 75 K the density is 6% smaller than at 50 K, and the specific heat about 30% larger, for instance). The same behavior is seen in plots of the calculated temperature. In Fig. 8 we plot the curves of the temperatures obtained by the two techniques, at a small fluence 0.03 J/m^2 and two different times. We see that the agreement is very good, and that the maximum increase in the temperature is about 8 K. However, the same curves corresponding to a laser fluence of 0.1 J/m^2 differ about 50% (due mainly to the rapid increase of the specific heat with temperature).

At fluences higher than about 0.15 J/m^2 melting and vaporization occur, and the longitudinal-acoustic precursor arrival tend to displace to larger times. This can be expected from the fact that we can argue qualitatively that the acoustic signal produced by the pressure of the evaporated material

must be superimposed to the thermoelastic mechanism, producing an increase in the acoustic signal at later times^{1,4} (because vaporization begins for small laser fluences at the end of the laser pulse, and because the vaporization pressure takes a long time to drop off).

V. CONCLUSIONS

This work shows that it is possible to obtain quantitative information on acoustic waves produced by pulsed laser irradiation of a material, by means of a simple molecular dynamics simulation. There are, however, several aspects to take into account, including sample shape and size, and careful initial thermalization in order to get ride of background elastic oscillations.

We present results showing the expected longitudinal precursor shape, for several fluences, and discuss the influence on the observed pulse characteristics of the melting or ablation of the sample surface.

We also present numerical results of a standard thermoelastic model, in a one-dimensional geometry, demonstrating that very good agreement is obtained at low fluences between the molecular dynamics simulations and the thermoelasticity predictions, but that nonlinearities and temperature dependence of the physical parameters must be taken into account in order to predict accurately both maximum achieved temperatures and acoustic wave shape at higher fluences. A careful study of the temperature dependence of both the longitudinal- and transversal-acoustic wave speeds and of the thermal constants of the Lennard-Jones material is necessary to make a detailed nonlinear thermoelastic model, and to extend the present comparison to higher fluences.

This analysis, as well as the extension of the simple model presented to the case where there is ablation of the irradiated surface is currently in progress, and will be reported elsewhere.

*Electronic address: jetchev@dm.uba.ar

¹R. J. Dewhurst, D. A. Hutchins, S. B. Palmer, and C. B. Scruby, *J. Appl. Phys.* **53**, 4064 (1982).

²C. B. Scruby, R. J. Dewhurst, D. A. Hutchins, and S. B. Palmer, *J. Appl. Phys.* **51**, 6210 (1980).

³F. A. McDonald, *Appl. Phys. Lett.* **54**, 1504 (1989).

⁴F. V. Bunkin, Al. A. Kolomensky, V. G. Mikhalevich, *Lasers in Acoustics* (Harwood Academic, Chur, Switzerland, 1991).

⁵M. Mesaros, O. Martínez, G. M. Bilmes, and J. O. Tocho, *J. Appl. Phys.* **81**, 1014 (1997).

⁶M. Mesaros, O. Martínez, G. M. Bilmes, and J. O. Tocho, *An. Asoc. Quim. Argent.* **84**, 167 (1996).

⁷L. S. Gournay, *J. Acoust. Soc. Am.* **40**, 1322 (1966).

⁸V. Gusev, A. A. Kolomensky, and P. Hess, *Appl. Phys. A: Mater. Sci. Process.* **61A**, 285 (1995).

⁹F. V. Bunkin and V. M. Komissarov, *Akust. Zh.* **19**, 305 (1973) [*Sov. Phys. Acoust.* **19**, 203 (1973)].

¹⁰M. Ziv, *J. Acoust. Soc. Am.* **89**, 1556 (1991).

¹¹L. R. F. Rose, *J. Acoust. Soc. Am.* **75**, 723 (1984).

¹²M. Kasai, S. Fukushima, Y. Gohshi, T. Sawada, M. Ishioka, and M. Kaihara, *J. Appl. Phys.* **64**, 972 (1988).

¹³L. V. Zhilghei, P. B. S. Kodali, and B. J. Garrison, *J. Phys. Chem. B* **101**, 2028 (1997).

¹⁴S. J. Zhou, D. M. Beazley, P. S. Lomdahl, and B. L. Holian, *Phys. Rev. Lett.* **78**, 479 (1997).

¹⁵S. J. Zhou, D. L. Preston, P. S. Lomdahl, and D. M. Beazley, *Science* **279**, 1525 (1998).

¹⁶B. L. Holian and R. Ravelo, *Phys. Rev. B* **51**, 11 275 (1995).

¹⁷B. L. Holian and P. S. Lomdahl, *Science* **280**, 2085 (1998).

¹⁸L. Verlet, *Phys. Rev.* **159**, 98 (1967).

¹⁹D. C. Rapaport, *Comput. Phys. Rep.* **9**, 1 (1988).

²⁰J-P. Hansen and L. Verlet, *Phys. Rev.* **184**, 151 (1969).

²¹P. Gumbsch, S. J. Zhou, and B. L. Holian, *Phys. Rev. B* **55**, 3445 (1997).

²²J. Q. Broughton and G. H. Gilmer, *J. Chem. Phys.* **79**, 5095 (1983).

²³C. P. Flynn and R. S. Averback, *Phys. Rev. B* **38**, 7118 (1988).

²⁴M. W. Finnis, P. Agnew, and A. J. E. Foreman, *Phys. Rev. B* **44**, 567 (1991).

²⁵H. Hakkinen and Uzi Landman, *Phys. Rev. Lett.* **71**, 1023 (1993).

²⁶J. H. Brannon, J. R. Lankard, A. I. Baise, F. Burns, and J. Kaufman, *J. Appl. Phys.* **58**, 2036 (1985).

²⁷K. Schildebach, *Proc. SPIE* **1279**, 60 (1990).

²⁸G. D. Mahan, H. S. Cole, Y. S. Liu, and H. R. Philipp, *Appl. Phys. Lett.* **53**, 2377 (1988).

²⁹F. Enguehard and L. Bertrand, *J. Appl. Phys.* **82**, 1532 (1997).